Current Optics and Photonics

MS ID: 230053

Manuscript Type: Research Paper

Title: Numerical Analysis of Light Extraction Efficiency of a Core-Shell Nanorod Light-Emitting Diode

Keywords: Core-Shell Nanorod LED, FDTD analysis, Light Extraction Efficiency (LEE)

Abstract:
We present a detailed analysis of the light extraction efficiency (LEE) of the core-shell nanorod LED using finite-difference time-domain (FDTD) simulations. We found that the LEE has a deep dependence on source positions and polarization directions based on the calculated LEE results for every x and z position inside the core-shell nanorod structure. For the upper part (Pyramid) and the lower part (Sidewall) of the core-shell nanorod, the LEEs are different for Pyramid and Sidewall owing to total internal reflection (TIR) and the generated optical modes in the structure. As a result, the LEE of Sidewall is much larger than that of Pyramid. The averaged LEE of core-shell nanorod LED is also investigated with variable p-GaN thickness, n-GaN thickness, and height for the design guideline for the optimized LEE of core-shell nanorod LEDs.

Vol. *, No. *, Month Year, pp. *–*

Current Optics and Photonics

Regular Paper

Numerical Analysis of Light Extraction Efficiency of a Core-Shell Nanorod Light-Emitting Diode

Kangseok Kim†, Gijun Ju†, and Younghyun Kim*

[1]*Department of Photonics and Nanoelectronics, Hanyang University, Ansan 15588, Korea*

†*These authors contributed equally to this paper.*

We present a detailed analysis of the light extraction efficiency (LEE) of the core-shell nanorod LED using finite-difference time-domain (FDTD) simulations. We found that the LEE has a deep dependence on source positions and polarization directions based on the calculated LEE results for every x and z position inside the core-shell nanorod structure. For the upper part (Pyramid) and the lower part (Sidewall) of the core-shell nanorod, the LEEs are different for Pyramid and Sidewall owing to total internal reflection (TIR) and the generated optical modes in the structure. As a result, the LEE of Sidewall is much larger than that of Pyramid. The averaged LEE of core-shell nanorod LED is also investigated with variable p-GaN thickness, n-GaN thickness, and height for the design guideline for the optimized LEE of core-shell nanorod LEDs.

Keywords: Core-Shell Nanorod LED, FDTD analysis, Light Extraction Efficiency (LEE),
OCIS codes: (230.3670) Light-emitting diodes; (230.0230) Optical devices; (050.1755) Computational electromagnetic methods;

I. INTRODUCTION

With the advancement in display technology, an inorganic micro-LED has attracted great attention as a promising display light source because it promises lower power consumption, a longer life span, and faster response time compared to organic LEDs [1–3]. Recently, there has been much research to reduce the micro-LED size even further as the growing requirement for high resolution in the next-generation display such as virtual reality (VR) or augmented reality (AR) applications [4,5]. Even the technology roadmap continues to the nano-size LED not only for the further demands on display technology but also for the increase in device integration density [6,7]. In addition, the potential of the nano-scale LED has been growing for the more efficient electrical and optical performance of novel device architectures, like the nano-ring LED, nano-needle LED, and even nanorod LED compared to the conventional LEDs [8–10].

Gallium Nitride (GaN)-based LEDs, which have wide coverage of light-emitting colors through bandgap manipulation, have remarkably progressed over the last two decades since the first application of LEDs in the early 1990s [11,12]. However, in the conventional GaN-based LEDs, the performance is still restricted owing to the threading dislocation caused by the lattice mismatch between the GaN and the substrate, and the quantum-

*Corresponding author: younghyunkim@hanyang.ac.kr, ORCID 0000-0001-8072-1251

Color versions of one or more of the figures in this paper are available online.

confined Stark effect (QCSE) in multiple quantum well (MQW) [13–15]. This QCSE leads to a spatial separation of the electron and hole wave functions and a decline of the transition energy between them [15–18]. In terms of that, a core-shell nanorod structure, which was demonstrated in the reference [19,20], is considered a highly promising solution to avoid the degradation caused by the QCSE and threading dislocation resulting in high efficiency [21]. While the conventional planar LED has been grown to a *c*-plane, the GaN-based core-shell nanorod LED can be grown on a non-polar or semi-polar plane, leading it to be free from the internal polarization field [20,21]. Furthermore, an improvement of optical properties is also expected because the core-shell nanorod structure has an enlarged active area and reduced dislocation density due to a high aspect ratio and reduced influences of thermal and lattice mismatch, respectively [22–26].

As the conventional LED performance has been improved by maximizing the external quantum efficiency (EQE), it should also be developed for a highly efficient nano LED. The external quantum efficiency (EQE) is described below:

$$\eta_{EQE} = \eta_{IQE} \times \eta_{LEE} \quad , \tag{1}$$

, where η_{EQE} is how many photons emit to free space compared to total electrons injected into the LED. In Eq. (1), the EQE is the product of internal quantum efficiency (IQE) and light extraction efficiency (LEE). The LEE is defined as the proportion of the number of photons emitted to free space from the LED to the number of photons emitted from the active region inside the LED [27]. As can be seen in Eq. (1), LEE is considered one of the most important parameters to achieve high EQE. Since the LEE strongly depends on its structure, it is important to understand how the generated light or photons escape from the nanostructure so that it can be designed for high LEE.

The current white LEDs face several limitations due to the use of yellow phosphors, which result in color conversion loss, low color rendering index, and increased costs. The GaN-based core-shell nanorod white LED has emerged as a promising alternative to overcome these limitations [28,29], as it shows a broad Photoluminescence intensity due to the involvement of the pyramid top of the core-shell nanorod in longer wavelengths [29]. However, the lack of quantitative understanding of light extraction in the core-shell nanostructures is a growing concern that needs to be addressed. Our study aims to narrow this knowledge gap and contribute to the development of highly efficient next-generation display technology with tens of millions of nano LEDs, making it a timely and significant research endeavor.

II. SIMULATION METHOD

For the simulations in this study, we employed the commercially available FDTD simulation solver by Lumerical Inc [30]. The three-dimensional illustrations of GaN-based core-shell nanorod LED and its inside are shown in Fig. 1(a). The dipole source positions are also marked in the figure. At each position, a dipole source is considered in three directions of the *x*-, *y*-, and *z*-axis for the accurate simulation of the nanorod LED, in which the translational symmetry is not anymore maintained [31]. Since the surfaces of the hexagonally structured nanorod are symmetric and the surface is also bisymmetry, the LEE regarding half of one surface was simulated as shown in Fig. 1(a). We name the top of the core-shell nanorod structure

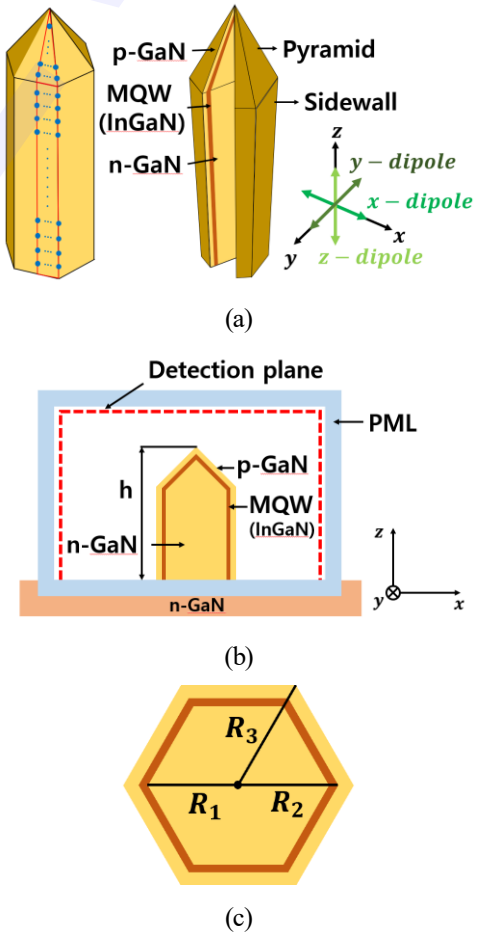

FIG. 1. (a) 3D schematic of core-shell nanorod for internal

configuration and dipole source positions marked on the surfaces. (b) side view and (c) cross-section of the GaN-based core-shell nanorod structure. FDTD simulation range enclosed by PML boundaries.

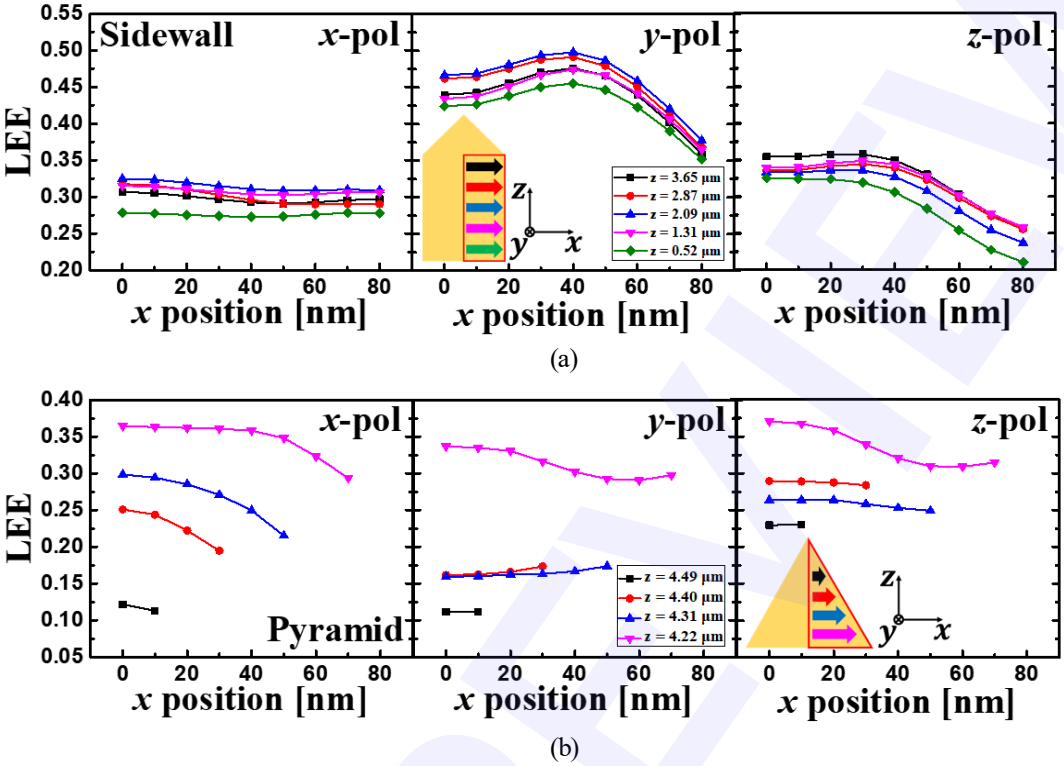

FIG. 2. LEE vs. source position in the (a) Sidewall or (b) Pyramid for the *x* position with dipole sources polarized in the *x*, *y*, and *z* directions.

"Pyramid" and the bottom of it "Sidewall". The FDTD simulations at each position on Sidewall and Pyramid were conducted by varying the dipole source positions along with *x*- and *z*-direction. On the other hand, the *y*-direction is neglected because of the very thin MQW layer thickness, typically a few tens of nanometer [32]. Fig. 1(b) shows a schematic side view of the core-shell nanorod structure and computational domain. The simulated core-shell nanorod LED structure is exposed to air and applied to the perfectly matched layers (PMLs) in all boundaries of the FDTD simulation domain so that propagating light is entirely absorbed in the PML. The Poynting vectors used in the LEE calculation are analyzed on the detection plane in PML as seen in Fig. 1(b).

The GaN-based core-shell nanorod LED grown on the n-GaN substrate consists of the n-GaN main rod (R_1 = 145 nm), an InGaN/GaN multiple-quantum-well (MQW) shell (R_2 = 175nm), the p-GaN shell (R_3 = 225 nm) outside of the rod, and the fixed height (h = 4.6 μm) as depicted in Fig. 1(c). The structure parameters were chosen considering the experimental demonstration [23]. The emitted wavelengths from a dipole source were set at 440 nm to 460 nm in the Sidewall and at 495 nm to 515 nm in the Pyramid [33]. The spectrum intensity of a dipole source is a Gaussian shape with each peak intensity at 450 nm, and 505 nm inthe Sidewall and Pyramid, respectively. Since the emission wavelengths are different depending on the In mole fraction in the MQW, it was set depending on the region. The effective refractive index of GaN is 2.48 and 2.42 as the emission wavelength ranges from 440 nm to 460 nm and from 495 nm to 515 nm, respectively [34]. The In mole fraction in the MQW shell is 10% in the Sidewall and 20% in the Pyramid [35]. The refractive index of InGaN/GaN active region in the Sidewall is 2.54 and 2.45 for the wavelength ranges of 440 nm to 460 nm and 495 nm to 515 nm, respectively [36]. In the Pyramid, the refractive index of the MQW is 2.62 and 2.68 for the same wavelength range [36]. The LEE at position (*x*, *y*, *z*) with each polarization in the MQW is calculated by the

$$T(f) = \frac{\frac{1}{2}\int_{monitor} Re(P(f))\cdot dS}{sourcepower(f)} \quad . \qquad (2)$$

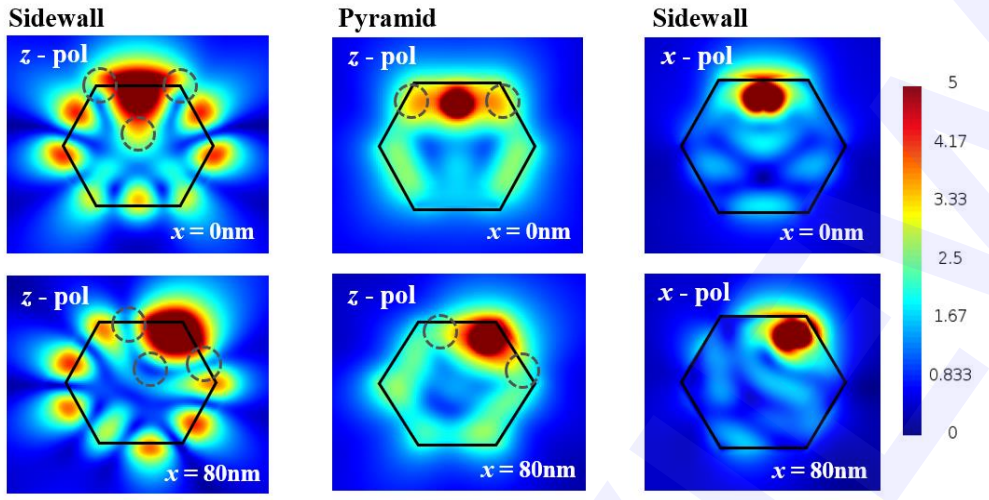

FIG. 3. (a), (b) Electric field intensity distribution when *z*-polarization is in the Sidewall and Pyramid respectively; (c) Electric field intensity distribution when x-polarization is in the Sidewall. The upper profile and the lower profile indicate when the dipole source is located at x=0 nm and x = 80nm, respectively.

, where $T(f)$ is the normalized transmission as a function of frequency and P is the Poynting vector, meaning that the amount of power transmitted through power monitors and profile monitors normalized to the source power is obtained.

III. RESULT AND DISCUSSION

Fig. 2(a) and 2(b) show the simulation results of the LEE as a function of x position for Sidewall and Pyramid, respectively. Three sources of *x*-, *y*-, and *z*-polarization of the LEE are plotted as a function of the x position from the left-hand to right-hand sides. For Sidewall in Fig. 2(a), the LEE of *x*-polarization slightly decreases with increasing x position but is almost constant at around 30%. The LEEs of *y*- and *z*-polarization vary from 35% to 50% and from 20% to 35%, respectively. The three polarizations show similar dependency in which the LEE decreases with an increase in the x position. For Pyramid in Fig. 2(b), the LEEs show a similar trend of decrease with an increase in x-position, but they show larger z-position dependency due to its geometrical effect compared to those of Sidewall.

The LEE depending on the dipole polarization and source position is highly related to the resonant optical modes inside core-shell nanorod, which influence the optical properties in the cavity. In terms of that, whispering gallery mode (WGM) is one of the resonant modes in nanorod cavity structure, arising from the interference with light circulating inside the curvature of the structure boundaries by total internal reflection [37,38]. WGMs is usually generated in circular structure or dome, but it is also formed even in hexagonal structure [38]. The position and size of WGMs are formed depending on the shape and size of the core structure. When a dipole source is positioned where the electric field is strongest due to the WGM's optical confinement, the emitted light travels along with the circumstance of the structure and escapes from it very slowly [37,38].

Fig. 3 shows the electric field intensity profile of the *x*-*y* plane. The top and bottom profiles are when the dipole is located at x = 0 nm and x = 80 nm, respectively. Fig. 3(a) presents the electric field intensity profile of the *x*-*y* plane when the dipole is on the Sidewall and oscillates in the *z*-direction. The light is more confined into the structure circularly due to the property of the WGM as mentioned earlier. In addition, similar results were observed for the *y*-polarization. Thus, it will be the root of the decrease of the LEE in the cases of *y*- and *z*-polarization in Fig. 2(a). Fig. 3(b) is a similar condition to Fig. 3(a), but the dipole is placed in Pyramid. The result shows that the emitted light is more confined along with the increasing x position. Hence, the LEE is reduced as shown in Fig. 2(b). The difference in the WGM between Sidewall and Pyramid is that the Sidewall shows a clear mode while Pyramid shows a blurred mode, meaning that the WGM is formed stronger in the Sidewall than in the Pyramid. Therefore, the decrease

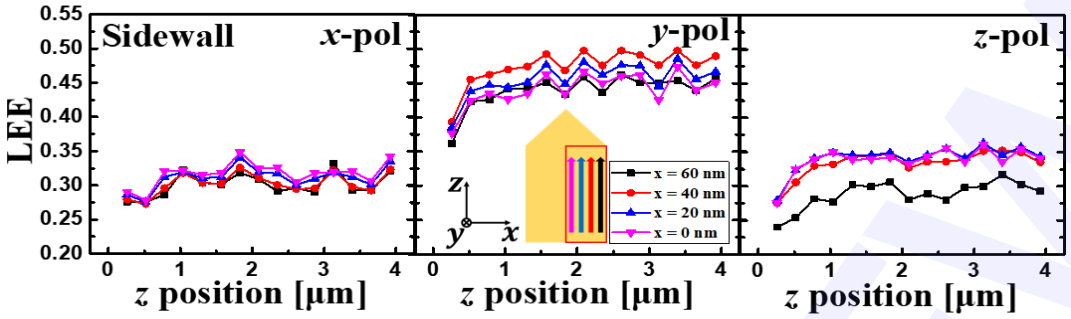

(a)

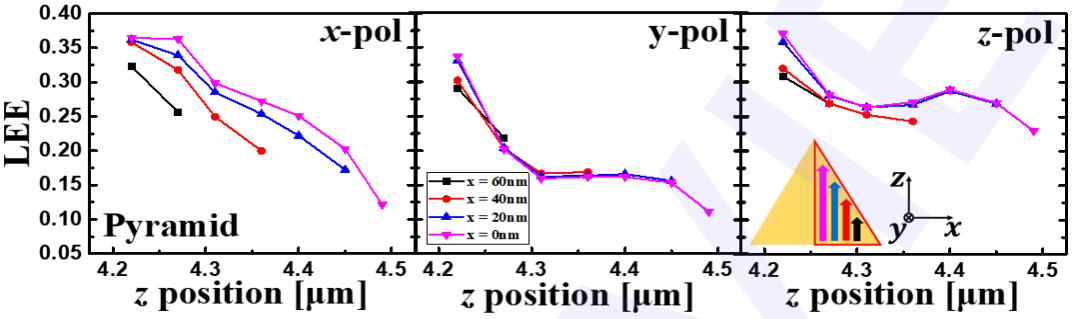

(b)

FIG. 4. LEE vs source position in the (a) Sidewall or (b) Pyramid for the z position with dipole sources polarized in the *x*,*y*, and *z* direction.

in LEE for Sidewall is larger than that in LEE for Pyramid. Fig. 3(c) shows the electric field intensity profile of x-polarization. Unlike, y- and z- polarization, the WGM is not observed regardless of the dipole position on the *x*-axis. Itwill be a reason for the almost constant LEE with variable *x* positions, mentioned in Fig. 2(a).

Fig. 4(a) and 4(b) show the LEE results as a function of the *z* position for Sidewall and Pyramid, respectively. The three figures are for *x*-, *y*-, and *z*-polarization in order from left to right. In Fig. 4(a), the LEEs of the three polarizations fluctuate along with the *z* direction. They are roughly 30%, 45%, and 30% for *x*-, *y*-, and *z*-polarization, respectively. Furthermore, the fluctuation variation between a maximum and minimum value is approximately 2.5%. The LEE of *y*-polarization is higher than that of *x*- and *z*-polarization, like the results in Fig. 2(a). In Fig. 4(b), the results are simulated with the same conditions as shown in Fig. 4(a), but the dipole source is located at the center of the MQW in Pyramid. As increasing *z* position, the LEEs for all polarizations significantly decrease.

The refractive index of GaN is much larger than that of air, so multi modes can be induced in a core-shell nanorod

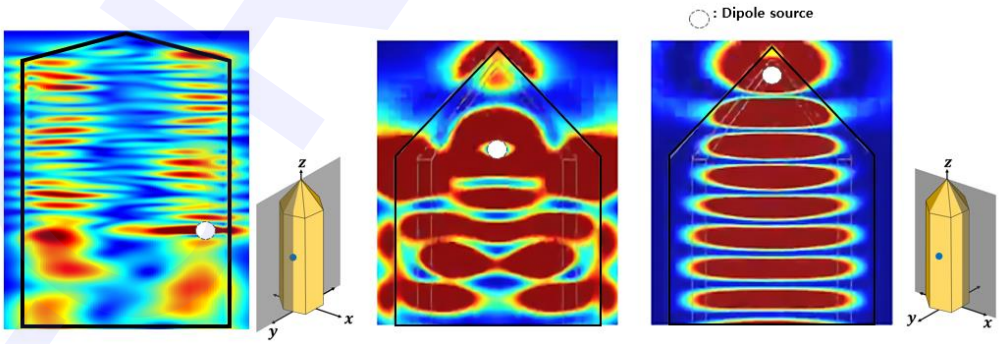

(a) (b)

FIG. 5. (a) Electric field intensity distribution of the *y*-*z* plane; (b) electric field intensity distribution of the *x*-*z* plane with the dipole sources on the bottom (z = 4.22 μm) and top (z = 4.49 μm) of the Pyramid.

structure like a waveguide. These multi modes lead to the formation of a specific propagating mode owing to the difference in inherent speed. When light is coupled with the propagating mode, it can be relatively easy to escape the core-shell nanorod structure. In other words, a high or low LEE appears when the dipole source position matches the high or low magnitude of the mode [31]. In Fig. 5(a), the electric field distribution viewed from the center of the *x*-axis shows the vertical propagation mode when the dipole is placed on the Sidewall. The vertical propagation mode formed a periodical array with intense domains, resulting in the fluctuation of the LEE for the *z*-direction as mentioned above.

To investigate the significant decrease in the LEE depending on the *z*-position for Pyramid in Fig. 4(b), the electric field intensity profiles of the *x*-*z* plane were analyzed with the two dipole source positions of z = 4.22 μm and 4.49 μm, near the bottom and top of Pyramid, respectively in Fig. 5(b). It reveals that the light can escape the structure through the Pyramid and the top of the Sidewall in the left-hand distribution, while the light is confined inside the nanorod except in adjacent regions of the peak of the Pyramid from the right-hand distribution. This result would be also explained by the Total internal reflection (TIR) as the dipole source's *z*-position increased. Using the formula of the TIR, $\theta_c = \sin^{-1}(n_t/n_i)$, the angle is obtained to 24.4 degrees. The refraction indices of GaN and air were set at 2.42 and 1. The thickness of InGaN is too thin and the indices difference is too low to be considered. Considering the calculated angle of TIR, the emitted light at the top region is more reflected than that at the bottom region as the z position of the dipole source goes up. The results are identical to the profile analysis in Fig. 5(b), thus, resulting in the decline of the LEE in accordance with the height of the Pyramid.

Fig. 6 shows the LEE distribution in Pyramid and Sidewall for *x*-, *y*-, *z*-polarization, and their total. As mentioned earlier, Sidewall shows larger LEE values compared to Pyramid for all polarizations. In addition, the *y*-polarized light shows the highest LEE for Sidewall but the

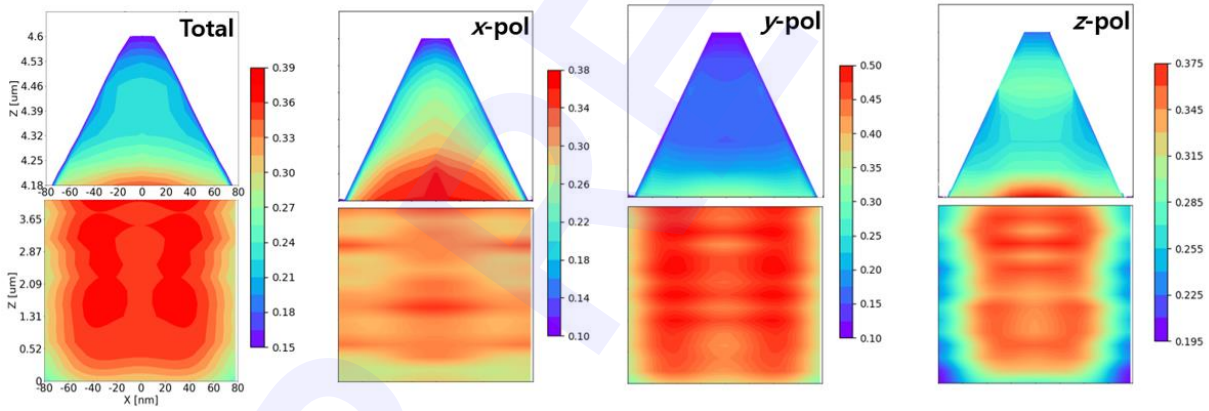

FIG. 6. LEE dimensional distribution of the whole, *x*-polarization, *y*-polarization, and *z*-polarization from left.

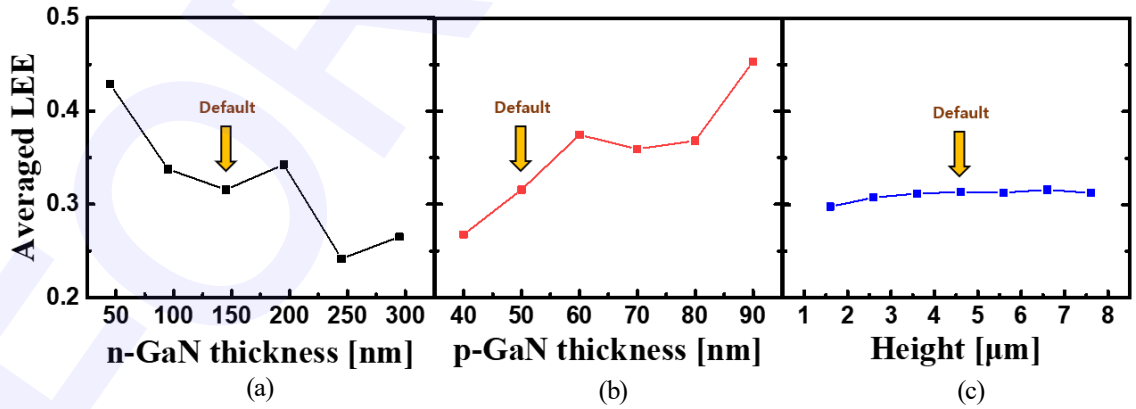

FIG. 7. The averaged LEE is plotted as a function of (a) n-GaN thickness, (b) p-GaN thickness, and (c) height for optimization. The fundamental structure of our study is expressed as default.

lowest for Pyramid. It suggests that Sidewall and *y* polarization are important design considerations for highly efficient core-shell nanorod LEDs.

We also explored the averaged LEE considering important parameters of n-GaN thickness, p-GaN thickness, and height for design optimization guidelines. The LEE was averaged from the whole positions and polarization. Fig. 7 shows the averaged LEE as a function of n-GaN thickness, p-GaN thickness, and height. The averaged LEE has the opposite tendency for the n-GaN thickness in Fig. 7(a) and p-GaN thick We also explored the averaged LEE considering important parameters of n-GaN thickness, p-GaN thickness, and height for design optimization guidelines. The LEE was averaged from the whole positions and polarization. Fig. 7 shows the averaged LEE as a function of n-GaN thickness, p-GaN thickness, and height. The averaged LEE has the opposite tendency for the n-GaN thickness in Fig. 7(a) and p-GaN thickness in Fig. 7(b). Their tendency would attribute to the shift of the relative MQW position. As the n-GaN thickness decrease, the light can easily escape due to the weak WGM. Similarly, as the p-GaN thickness increase, the longer distance between the dipole source and the air shrinks the WGM so that more light can ness in Fig. 7(b). Their tendency would attribute to the shift of the relative MQW position. As the n-GaN thickness decrease, the light can easily escape due to the weak WGM. Similarly, as the p-GaN thickness increase, the longer distance between the dipole source and the air shrinks the WGM so that more light can escape the core-shell nanorod structure. Although height is an important parameter determining active area, there is no significant change in the averaged LEE as shown in Fig. 7(c). It will be the same reason as discussed in Fig. 4(a) because the height is along with the *z*-direction.

As a result, we suggest the optimum core-shell nanorod LED with thin n-GaN thickness and thick p-GaN thickness so that the MQW is positioned as far from the surface as possible due to the relationship between the averaged LEE and the WGM. Also, when one designs the height of the core-shell nanorod LED, the active light-emitting area will only be needed to consider assuming a constant LEE.

II. CONCLUSION

In this study, we investigated the LEE in GaN-based core-shell nanorod LED structure using the FDTD simulation. It was revealed that the LEE has a deep dependence on source positions and polarization directions based on the calculated LEE results for every *x* and *z* position inside the core-shell nanorod structure. For Pyramid and Sidewall of the core-shell nanorod, the LEEs are different owing to total internal reflection (TIR) and the generated optical modes in the structure. Consequently, the LEE of Sidewall is much larger than that of Pyramid. The averaged LEE of core-shell nanorod LED is also investigated with variable p-GaN thickness, n-GaN thickness, and height for the design guideline for the optimized LEE of core-shell nanorod LEDs.

ACKNOWLEDGMENTS

This research was supported by the Technology Innovation Program (20015909) through the Korea Evaluation Institute of Industrial Technology (KEIT), funded by the Ministry of Trade, Industry & Energy (MOTIE, Korea). This work was supported by the National Research Foundation of Korea(NRF) grant funded by the Korea government(MSIT) (No. 2022K1A3A1A79090726). This work was supported by the National Research Foundation of Korea(NRF) grant funded by the Korea government(MSIT) (No. 2021R1G1A1091912).

REFERENCES

1. Chen, Zhen, Shuke Yan, and Cameron Danesh. "MicroLED technologies and applications: characteristics, fabrication, progress, and challenges." Journal of Physics D: Applied Physics **54.12** 1-34 (2021).
2. Liu, Zhaojun, et al. "Micro-light-emitting diodes with quantum dots in display technology." Light: Science & Applications **9.1** 1-23 (2020).
3. Anwar, Abdur Rehman, et al. "Recent Progress in Micro-LED-Based Display Technologies." Laser & Photonics Reviews **16.6** 1-20 (2022).
4. Gong, Zheng, et al. "Size-dependent light output, spectral shift, and self-heating of 400 nm InGaN light-emitting diodes." Journal of Applied Physics **107.1** 1-20 (2010).
5. Xiong, Jianghao, et al. "Augmented reality and virtual reality displays: emerging technologies and future perspectives." Light: Science & Applications **10.1** 1-30 (2021).
6. Perlman, Harel, Tsion Eisenfeld, and Avi Karsenty. "Performance enhancement and applications review of nano light emitting device (LED)." Nanomaterials **11.1** 1-25 (2020).
7. A. Waag, X. Wang, S. Fündling, J. Ledig, M. Erenburg, R. Neumann, M. Al Suleiman, S. Merzsch, J. Wei, S. Li, H. H. Wehmann, W. Bergbauer, M. Straßburg, A. Trampert, U. Jahn, and H. Riechert, "The nanorod approach: GaN NanoLEDs for solid state lighting," Phys. Status Solidi Curr. Top. Solid State Phys. **8**, 2296–2301 (2011).
8. J. Bai, Q. Wang, and T. Wang, "Greatly enhanced performance of InGaN/GaN nanorod light emitting diodes,"

Phys. Status Solidi Appl. Mater. Sci. **209**, 477–480 (2012).
9. S. W. Wang, K. Bin Hong, Y. L. Tsai, C. H. Teng, A. J. Tzou, Y. C. Chu, P. T. Lee, P. C. Ku, C. C. Lin, and H. C. Kuo, "Wavelength tunable InGaN/GaN nano-ring LEDs via nano-sphere lithography," Sci. Rep. **7**, 1–7 (2017).
10. L. C. Chuang, F. G. Sedgwick, R. Chen, W. S. Ko, M. Moewe, K. W. Ng, T. T. D. Tran, and C. Chang-Hasnain, "GaAs-based nanoneedle light emitting diode and avalanche photodiode monolithically integrated on a silicon substrate," Nano Lett. **11**, 385–390 (2011).
11. P. Pust, P. J. Schmidt, and W. Schnick, "A revolution in lighting," Nat. Mater. **14**, 454–458 (2015).
12. I. Akasaki, "Fascinated journeys into blue light," Int. J. Mod. Phys. B **29**, 7–37 (2015).
13. Lu, Chih-Feng, Chi-Feng Huang, and C. C. Yang. "Reduced blue shift in screening the quantum-confined stark effect of an InGaN/GaN quantum well with the prestrained growth of a light-emitting diode." Quantum Electronics and Laser Science Conference. Optica Publishing Group, paper JThA64. 14-15 (2008)
14. K. Pieniak, M. Chlipala, H. Turski, W. Trzeciakowski, G. Muziol, G. Staszczak, A. Kafar, I. Makarowa, E. Grzanka, S. Grzanka, C. Skierbiszewski, and T. Suski, "Quantum-confined Stark effect and mechanisms of its screening in InGaN/GaN light-emitting diodes with a tunnel junction," Opt. Express **29**, 1824-1837 (2021).
15. S. Zhu, S. Lin, J. Li, Z. Yu, H. Cao, C. Yang, J. Li, and L. Zhao, "Influence of quantum confined Stark effect and carrier localization effect on modulation bandwidth for GaN-based LEDs," Appl. Phys. Lett. **111**, 1-5 (2017).
16. Ambacher, O., et al. "Pyroelectric properties of Al (In) GaN/GaN hetero-and quantum well structures." Journal of physics: condensed matter **14.13** 3399-3434 (2002).
17. Miller, David AB, et al. "Band-edge electroabsorption in quantum well structures: The quantum-confined Stark effect." Physical Review Letters **53.22** 2173-2176 (1984).
18. Takeuchi, Tetsuya, et al. "Quantum-confined Stark effect due to piezoelectric fields in GaInN strained quantum wells." Japanese Journal of Applied Physics **36.4A** 1824-1837 (1997).
19. Robin, Y., et al. "Insight into the performance of multi-color InGaN/GaN nanorod light emitting diodes." Scientific Reports **8.1** 1-8 (2018).
20. Le Boulbar, E. D., et al. "Facet recovery and light emission from GaN/InGaN/GaN core-shell structures grown by metal organic vapour phase epitaxy on etched GaN nanorod arrays." Journal of Applied Physics **114.9** 1-10 (2013).
21. S. Li and A. Waag, "GaN based nanorods for solid state lighting," J. Appl. Phys. **111**, 1-23 (2012).
22. Jung, Byung Oh, et al. "Emission characteristics of InGaN/GaN core-shell nanorods embedded in a 3D light-emitting diode." Nanoscale Research Letters **11.1** 1-10 (2016).
23. Wang, Xue, et al. "Continuous-flow MOVPE of Ga-polar GaN column arrays and core–shell LED structures." Crystal growth & design **13.8** 3475-3480 (2013).
24. Tchernycheva, M., et al. "Core–shell InGaN/GaN nanowire light emitting diodes analyzed by electron beam induced current microscopy and cathodoluminescence mapping." Nanoscale **7.27** 11692-11701 (2015).
25. Vogt, Angelina, et al. "Recombination dynamics in planar and three-dimensional InGaN/GaN light emitting diode structures." Journal of Materials Research **32.13** 2456-2463 (2017).
26. Ryu, Han-Youl. "Effect of internal polarization fields in InGaN/GaN multiple-quantum wells on the efficiency of blue light-emitting diodes." Japanese Journal of Applied Physics **51.9S2** 1-4 (2012).
27. Shim, Jong-In, and Dong-Soo Shin. "Measuring the internal quantum efficiency of light-emitting diodes: Towards accurate and reliable room-temperature characterization." Nanophotonics **7.10** 1601-1615 (2018).
28. Evropeitsev, Evgenii A., et al. "State-of-the-art and prospects for intense red radiation from core–shell InGaN/GaN nanorods." Scientific Reports **10.1** 1-10 (2020).
29. Kim, Je-Hyung, et al. "Toward highly radiative white light emitting nanostructures: a new approach to dislocation-eliminated GaN/InGaN core–shell nanostructures with a negligible polarization field." Nanoscale **6.23** 14213-14220 (2014).
30. Lumerical Solution Inc., "FDTD Solution, A Commercial Professional Software," Lumerical Solution Inc., Vancouver, Canada. http://www.lumerical.com.
31. Ryu, Han-Youl. "Evaluation of light extraction efficiency of GaN-based nanorod light-emitting diodes by averaging over source positions and polarizations." Crystals **8.1** 1-8 (2018).
32. Huang, Huamao, et al. "Enhanced light output of dipole source in GaN-based nanorod light-emitting diodes by silver localized surface plasmon." Journal of Nanomaterials **2014** 1-8 (2014).
33. Riley, James R., et al. "Three-dimensional mapping of quantum wells in a GaN/InGaN core–shell nanowire light-emitting diode array." Nano letters **13.9** 4317-4325 (2013).
34. Adachi, Sadao. *Optical constants of crystalline and amorphous semiconductors: numerical data and graphical information*. (Springer Science & Business Media, Kiryu-shi, Japan 2013).
35. Schubert, E. *Light-Emitting Diodes* 2nd ed. (Cambridge, New York, USA, 2006)
36. Chen, Zhen, Shuke Yan, and Cameron Danesh. "MicroLED technologies and applications: characteristics, fabrication, progress, and challenges." Journal of Physics D: Applied Physics **54.12** 1-34 (2021).
37. Nobis, Thomas, and Marius Grundmann. "Low-order optical whispering-gallery modes in hexagonal nanocavities." Physical Review A **72.6** 1-11 (2005).
38. Wang, Zhihuan, and Bahram Nabet. "Nanowire optoelectronics." Nanophotonics **4.4** 491-502 (2015).